THE JOURNAL OF PHYSICAL CHEMISTRY B

Article

Cite This: J. Phys. Chem. B 2019, 123, 9481−9490

pubs.acs.org/JPCB

Structural Changes in Wormlike Micelles on the Incorporation of Small Photoswitchable Molecules

Natalia Rincón-Londoño,[†] Antonio Tavera-Vázquez,[†,§] Cristina Garza,[†] Nuria Esturau-Escofet,[‡] Anna Kozina,[‡] and Rolando Castillo*[,†]

[†]Instituto de Fisica, Universidad Nacional Autónoma de México, P.O. Box 20-364, 01000 Mexico City, Mexico

[‡]Instituto de Química, Universidad Nacional Autónoma de México, P.O. Box 70-213, 04510 Mexico City, Mexico

Supporting Information

ABSTRACT: Chromophores susceptible to light-induced trans−cis isomerization embedded in cylindrical micelles can modify micelles and their light-responsive performance. A small chromophore (4-(phenylazo)benzoate ion) is embedded in cylindrical micelles made of cetyltrimethylammonium bromide (CTAB) and sodium salicylate (NaSal) in water. The microstructure is examined by scanning electron microscopy (SEM) and nuclear magnetic resonance (NMR). Rheological behavior and the length scales of the micellar network are determined by rheology and microrheology. The chromophore substantially modifies the micelles even without UV irradiation. The larger is the chromophore concentration, the smaller is the micellar length. Additional length scales of the micellar network do not substantially vary even when NaCl is added. Chromophore incorporation also modifies the rheology of the micellar solution, although gradient shear banding is preserved. Viscosity decreases as the chromophore concentration increases, and viscoelastic spectra are modified, but when they are correctly rescaled, they can be superimposed. The addition of the chromophore makes the fluids more Maxwellian, particularly when NaCl is also added. When the chromophore is incorporated into the micelles, there is a response after UV irradiation, although it does not produce a significant rheological change.

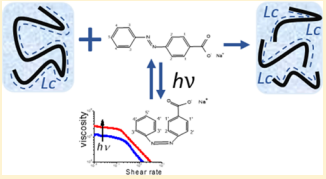

1. INTRODUCTION

Under specific thermodynamic conditions, such as temperature, concentration, and ionic strength, amphiphiles can assemble in spherical micelles, vesicles, and lamellae or grow to form long tubular flexible micelles forming an entangled network. The preferred morphology is fixed by the spontaneous curvature of the assembly that is determined by the most efficient packing of the amphiphiles in the involved aggregates. In particular, wormlike micelles (WLMs) have attracted considerable interest over the last 30 years in fundamental research, as well as in practical applications due to their unique properties.[1,2] WLMs have been used in oil fields, district heating and cooling, daily care products, hybrid materials, etc.[3,4]

In WLMs, energy is optimized when the curvature is uniform everywhere forming extended linear structures. Nevertheless, a degree of randomness is introduced in the system through bending the cylindrical micelles because of conformational entropy or through topological defects, such as end caps or branch junction points. Entropic gain associated with end caps is more important than those of branch points.[5] If the energy scission of a WLM (the energy required to form two end caps from an infinite cylinder) is large enough, linear micelles may become very long and entangled, as when the ionic strength of the media increases. Lowering the scission energy makes the total contour length of the micelles shorter; consequently, the number of micelles increases, as well as entropy. This balance determines the WLM contour length.[5] The number of possible configurations increases by branch junction points, enabling percolation that can form extended micellar networks that lead instead to multiconnected than to entangled networks of giant micelles.[5] Maxwell-like behavior is followed by most of the WLM solutions at low and intermediate frequencies, i.e., a single relaxation dominates the viscoelastic modulus that can be written as $G(t) = G_o e^{-t/\tau}$. The instantaneous shear modulus, G_o, and the relaxation time, τ, depend on surfactant concentration, temperature, and ionic force of the media. The modulus, $G(t)$, in the frequency domain can be expressed through the complex modulus $G^*(\omega) = G'(\omega) + iG''(\omega)$; $G^*(\omega) = i\omega \int_0^\infty G(t)\, e^{-i\omega t}\, dt$.[6] The real part is the elastic (storage) modulus in phase with the applied shear strain, γ. The imaginary part corresponds to the viscous (loss) modulus in phase with the shear rate, $\dot{\gamma}$.

Recently, a particular kind of WLMs has attracted attention because of their fast-response adaptative conditions (smart).[7,8] The macroscopic properties of these micellar solutions can undergo, on demand, an instantaneous and radical change in response due to an external stimulus, as the light is a noninvasive trigger, cheap, and readily available that can be directed at a precise spatial location. Light can be used as a trigger to change WLMs to be light-responsive if a suitable chromophore susceptible to a light-induced trans−cis isomerization is embedded in them. Isomerization can modify the packing of surfactant molecules inside aggregates, and it drives

Received: July 30, 2019
Revised: September 24, 2019
Published: October 9, 2019

DOI: 10.1021/acs.jpcb.9b07276
J. Phys. Chem. B 2019, 123, 9481−9490

micellar transitions from WLMs to other structures or modify their length. Consequently, some properties could be tuned, such as viscoelasticity. Azobenzene and its derivatives have played a significant role to control the rheological properties of WLM solutions. As examples, we can mention several systems where 4-(phenylazo)benzoate ion ($PhazoBCOO^-$) is the chromophore, which is combined with different micelle-forming compounds as (a) 1-hexadecyl-3-methylimidazolium bromide,[9] where the authors report that upon UV irradiation the WLMs become longer and entangled, exhibiting a high viscosity due to photoisomerization of the chromophore. (b) Erucyl bis(2-hydroxyethyl)methylammonium chloride[10] that self-assembles into low-viscosity unilamellar vesicles, and upon exposure to UV light, the chromophore undergoes photoisomerization, which alters its geometry and the system self-assembles into WLMs. (c) CTAB solutions that induce a WLM to vesicle transition with a maximum zero-shear viscosity at $[PhazoBCOO^-]/[CTAB] = 0.65$.[11] Here, the authors do not report photosensitivity. Other chromophores have also been used; some examples can be mentioned: (a) *trans*-2,4,4′-trihydroxychalcone mixed with CTAB and salicylic acid presents limited rheological changes with UV irradiation.[12] (b) The azobenzene-modified cationic surfactant 4-butylazobenzene-4′-(oxyethyl)-trimethylammonium bromide with CTAB and NaSal presents a significant viscoelastic change after UV irradiation.[13] (c) Tu and co-workers have studied the UV-responsive behavior of different supramolecular assemblies with different morphologies made of cationic Gemini surfactants and different photosensitive cinnamate derivatives, showing a wide variety of possibilities to modify the rheological response in smart fluids.[14−16]

This paper aims to study how a small chromophore as $PhazoBCOO^-$, where UV induces a trans−cis isomerization, interacts with well-known giant cylindrical micelle building blocks, as CTAB and NaSal in water solution. Several questions may arise: is $PhazoBCOO^-$ incorporated into the WLMs? Does the incorporation of $PhazoBCOO^-$ modify the micelle contour length? Are the length scales of the WLM micellar network in the solution modified? Does NaCl addition make the micelles grow in WLM solutions with the chromophore? What is the final consequence of $PhazoBCOO^-$ incorporation on the rheological behavior of the fluid? Is this chromophore able to modify the rheology of the micellar system through UV irradiation via trans−cis isomerization? These questions are essential to understand why some photoswitchable molecules work; meanwhile, others, with great potential to modify the rheology of WLM solutions after UV irradiation, do not work effectively. This report is the first of a series devoted to studying how chromophores interact with WLMs because embedding them in micelles is a necessary but not a sufficient condition to have a photoresponsive solution.

2. EXPERIMENTAL SECTION

2.1. Materials. Cetyltrimethylammonium bromide (CTAB, purity >99%) was acquired from Fluka (Switzerland); 4-(phenylazo)benzoic acid ($PhazoBCOO^- H^+$, purity >98%) was from TCI Tokyo Chemical (Japan); and sodium salicylate (NaSal, purity 99.5%), sodium chloride (NaCl, purity >99%), and sodium hydroxide (NaOH ≥97%) were from Sigma-Aldrich (Canada). Reactives were used as received. All samples were prepared with ultrapure deionized water (Nanopure).

2.2. Sample Preparation. $PhazoBCOO^- H^+$ was solubilized in deionized water to reach several concentrations that we denoted as C_{AZO}, of 5, 10, 15, and 20 mM, at pH 12 to form the $PhazoBCOO^-$; pH was fixed with the aid of a NaOH solution. These samples were stirred and heated up to 40 °C, and then CTAB and NaSal were added to reach specified concentrations. At larger C_{AZO}, solutions present a phase separation. Mixtures were stirred for 24 h and left to relax for 48 h. The micellar solutions had a constant ratio of $R = 0.5$ ($R = [NaSal]/[CTAB]$) with $[CTAB] = 0.080$ M. The same procedure was followed to prepare a second set of solutions, where NaCl is added to reach a concentration of 0.1 M. It is important to note that there is a small extra contribution to the ionic strength of the media due to the addition of NaOH to reach pH = 12.

2.3. UV Light Irradiation. Samples were irradiated with an LED array light source 365 nm@31 mW (LUI365A, Thorlabs) for 1 h before the tests and during all rheological measurements.

2.4. Scanning Electron Microscopy (SEM). We used an extreme-resolution analytical field-emission SEM (JSM-7800F JEOL Ltd. Japan) working at low electron acceleration voltages on negatively stained samples of the systems under study. This instrument is equipped with scanning transmission electron microscope (STEM) mode and with detectors for secondary and backscattered electrons, as well as with a liquid nitrogen trap to avoid specimen overheating.

2.5. Grids for Electron Microscopy. We used standard TEM grids covered with collodion and carbon layers to deposit a few microliters of micellar solutions close to the overlap concentration, C^*. Then, the grid is placed on a filter paper, and a drop of phosphotungstic acid (∼1.5 wt %) is added to the sample. After the filter paper absorbs the excess of the solution, the sample is dried under ambient conditions. The sample on the grid is covered with a thin carbon layer to assure that it is conductive.

2.6. UV−Vis Spectroscopy. The UV−vis spectra of dilute water solutions of $PhazoBCOO^- H^+$ with NaOH at 3.0×10^{-4} M were obtained before and after UV irradiation, using an Evolution 300 Thermo Scientific spectrophotometer at room temperature.

2.7. ^{1}H NMR and ^{1}H−^{1}H COSY. ^{1}H NMR spectra and ^{1}H−^{1}H COSY were acquired on a Bruker AVANCE III HD 500 MHz, equipped with a 5 mm *z*-axis gradient BBFO probe at various temperatures. Samples were dissolved in D_2O (99.9%) (Sigma-Aldrich) and NaOD to reach pH = 12. NMR experiments were recorded using standard Bruker pulse sequences. NMR spectra were referenced to the water signal resonance at each temperature.

2.8. Rheological Measurements. Rheological measurements were performed with an MCR-702 TwinDrive rheometer (Anton Paar, Austria). Flow curves and oscillatory measurements were carried out in a cone-plate geometry (40 mm in diameter and 2° cone angle) with temperature control (±0.1 °C). A solvent trap with a quartz window was used to avoid water evaporation and to keep the sample irradiated during the measurements. The oscillation experiments were obtained in the linear regime.

2.9. Microrheology and Diffusive Wave Spectroscopy (DWS). The viscoelastic spectrum of a WLM solution can be extended to high frequencies (∼10^6 rad s^{-1}) using DWS. In microrheology, the mean square displacement (MSD or $\langle \Delta r^2(t) \rangle$), of particles embedded in a complex fluid can be

DOI: 10.1021/acs.jpcb.9b07276
J. Phys. Chem. B 2019, 123, 9481−9490

measured with DWS. The MSD can be related to $G^*(\omega)$ using a generalized Stokes–Einstein equation[17]

$$G^*(\omega) = G'(\omega) + iG''(\omega) = \frac{k_B T}{\pi r_o i\omega \Im\langle \Delta r^2(t)\rangle(\omega)}. \quad (1)$$

where $\Im$ is the unilateral Fourier transform, r_o is the particle diameter, ω is the angular frequency, k_B is the Boltzmann constant, and T is the temperature. Our DWS setup is described elsewhere.[18] The MSD of probe particles is determined by collecting their scattered light from a single speckle over a sufficiently long period, evaluating the time-averaged intensity autocorrelation function. The probe particles within the micellar liquid are placed in a slab-shaped cuvette with an optical path length $L \gg l^*$ and infinite transverse extent.[18] Here, l^* is the transport mean free path of light. DWS assumes that the fluid where the probe particles will be dispersed is entirely transparent to the incident light beam. Nevertheless, micellar solutions with azo-compounds absorb light, even at low concentrations. A correction has to be included to overcome this inconvenience, using the inverse adding-doubling method (IAD)[19,20] that is a procedure developed for optical parameter recovery, as the absorption lengths l_a and l^*. The input parameters come from three measurements: total reflectance, total transmittance, and collimated transmittance of light. The measured l_a allows us to correct the intensity autocorrelation function and hence MSD of the tracers, using the method developed by Sarmiento-Gomez et al.[21] The experimental MSD curve is best fitted with a model curve proposed by Bellour et al.[22] for particles immersed in WLM solutions

$$\Delta r^2(t) = 6\delta^2\left(1 - e^{-\left(\frac{D_0}{\delta^2}t\right)^{\alpha}}\right)^{1/\alpha}\left(1 + \frac{D_m}{\delta^2}t\right) \quad (2)$$

where $6\delta^2$ measures the plateau of $\langle\Delta r^2(t)\rangle$ vs t curve, D_o and D_m are the diffusion coefficients for particles in the solvent at infinite dilution and at long times, respectively. Finally, each component of $G^*(\omega)$ is obtained using the fitting curve in eq 1. Microrheology contributes to estimating the most important characteristic lengths of the WLM network, using approximate relations coming from theory. At time scales shorter than those of WLM breakage time corresponding to high frequencies, the Maxwellian stress relaxation processes are fundamentally frozen; here, WLMs behave like semiflexible polymer chains. Stress relaxes first dominated by the Rouse–Zimm modes and then by the internal relaxation of Kuhn segments. At those frequencies, $G^*(\omega)$ exhibits a power-law behavior, $|G^*| \sim \omega^{\nu}$, with the exponent $\nu \sim 5/9$ in the Rouse–Zimm regime, which changes to $\nu \sim 3/4$, where the internal bending modes of Kuhn segments dominate. This change occurs at a frequency ω_0 ($\omega_0 \approx k_B T/8\eta_s l_p^3$, η_s is the solvent viscosity)[23] that corresponds to the shortest relaxation time in the Rouse–Zimm spectrum. From ω_0 coming from the slope change in $|G^*(\omega)|$, l_p can be obtained, and other characteristic lengths of major interest to understand the structure and dynamics of WLMs can be evaluated, for example, the total contour length, L_c, the persistence length, l_p, the entanglement length, l_e, and the mesh size ξ. The WLM network mesh size can be estimated in the loose entanglement regime with $\xi \cong \left(A\frac{k_B T}{G_o}\right)^{1/3}$, where the prefactor $A = 9.75$ is a correction recently given.[24] In the same way, l_e can be computed using $l_e = \xi^{5/3}/l_p^{2/3}$.[25] The total contour length can be estimated from $G''_{min}/G_0 \cong (l_e/L_C)^{0.8}$, which comes from incorporating breathing and high-frequency Rouse modes; the exponent is a correction given by Granek.[26] Here, G''_{min} is the local minimum of $G''(\omega)$ after the first crossing between $G'(\omega)$ and $G''(\omega)$. The ratio of the entanglement length to the persistence length, $\alpha_e = l_e/l_p$, can also be obtained, and it is useful to determine if the system is in the loose ($\alpha_e > 2$) or tight entanglement regime ($\alpha_e < 1$).[24]

3. RESULTS AND DISCUSSION

CTAB/NaSal self-assemble in WLMs[27] and, apparently, are stable enough to include the PhazoBCOO$^-$ into the tubular micelle since these WLMs can incorporate larger azobenzene derivatives.[13,28,29] Figure 1 shows negative staining micro-

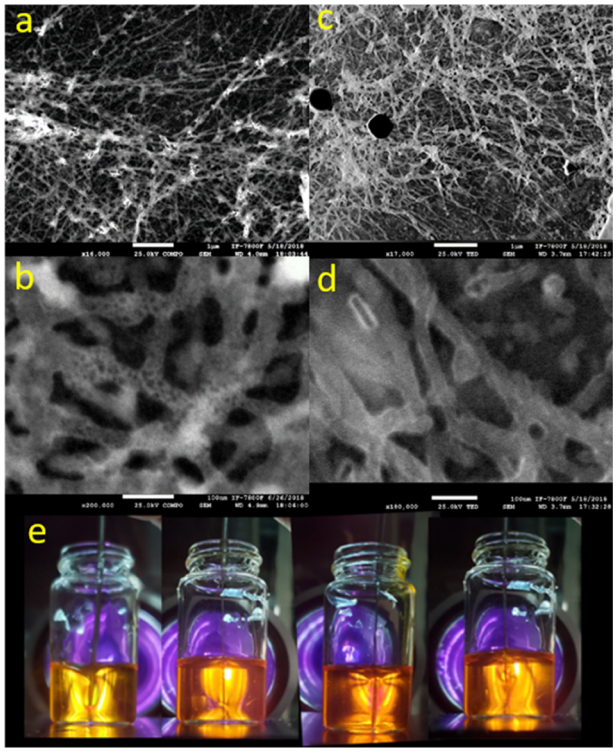

Figure 1. Direct observation of WLM bundles made of CTAB/NaSal/PhazoBCOO$^-$ (C_{CTAB} = 4 mM, R = 0.5) backscattered electrons: (a) 16 000×, bar = 1 μm, (b) 200 000×, bar = 100 nm. STEM-in-SEM: (c) 17 000×, bar = 1 μm, and (d) 180 000×, bar = 100 nm. (e) Birefringence in yellow micellar solutions between crossed polarizers under shear due to a slowly dipped spatula at C_{AZO} = 5, 10, 15, and 20 mM (from left to right).

graphs obtained by SEM of dilute micellar solutions made of CTAB/NaSal/PhazoBCOO$^-$. Tubular structures as bundles are observed. At the largest accessible amplification, one can see that the tubular structures are made of bundles of thinner tubular morphologies, probably individual WLMs. At rest, the micellar solutions are not birefringent. However, as shown in Figure 1e, birefringence appears when they are sheared, which is typical behavior of WLM solutions.

3.1. Trans–Cis Isomerization. Figure 2 presents the isomerization reaction, as well as the UV–vis absorbance spectra of PhazoBCOO$^-$ Na$^+$ (3×10^{-4} M) in water solution at pH = 12. As other azobenzene derivatives, PhazoBCOO$^-$ has two transitions: the first one, $\pi \rightarrow \pi^*$, occurs at 325 nm and the second one, n $\rightarrow \pi^*$, at 420 nm. When the sample is

DOI: 10.1021/acs.jpcb.9b07276
J. Phys. Chem. B 2019, 123, 9481–9490

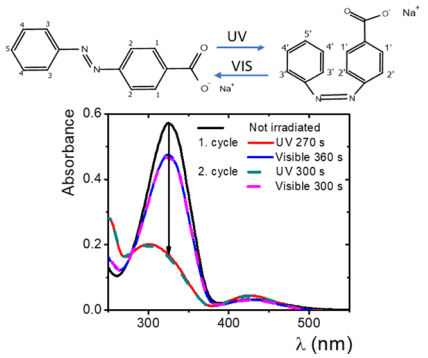

Figure 2. Upper panel: trans−cis isomerization with the proton numbering to be used below. Lower panel: UV−vis absorbance spectra for PhazoBCOO$^-$ (pH = 12), for two cycles of irradiation using different irradiation times.

UV-irradiated for 270 s, the band at 325 nm decreases and the one at 420 nm slightly increases. This behavior is typical for trans−cis isomerization processes.[9,10] On white light irradiation (260 s), the transition goes backward, although it does not reach the initial absorbance of the sample not previously irradiated. The same occurs for longer irradiation times.

3.2. ^{1}H NMR and ^{1}H−^{1}H COSY. Figure 3 presents the ^{1}H NMR spectra for (a) pure PhazoBCOO$^-$ H$^+$ (10 mM, pH = 12) and (f) pure NaSal (20 mM) in deuterated water. Their signals will be used as a reference to describe the spectra of these compounds incorporated in the WLMs.[30,31] Signal numbering in Figure 3a,f corresponds to protons shown in Figure 2 and the inset of Figure 3, respectively. In spectrum (a), there are signals for both trans and cis isomers as reported in the previous literature.[9,10] Spectrum (f) presents narrow peaks for S1, S3, and S2, S4 protons.[32] The spectrum (b) corresponds to WLMs without the chromophore (C_{CTAB} = 80 mM, R = 0.5). Here, the proton signals of NaSal are broader and shifted to lower frequencies with respect to the pure NaSal in water. The protons of CTAB are observed at low frequencies (1−2 ppm) and are irrelevant for the discussion. The spectra (c), (d), and (e) are for WLMs with PhazoBCOO$^-$ at C_{AZO} = 10, 15, and 20 mM (C_{CTAB} = 80 mM, R = 0.5, pH = 12), respectively. Here, S2, S4, and S3 signals are similar to those of spectrum (b), although gradually shifted to lower δ (lower frequencies with respect to spectrum f) indicating less electronegative surrounding. This reveals that these protons are incorporated deeper into the hydrocarbon tails of micelles. A small shift of S1 proton implies a similar environment of the equivalent proton in NaSal in water. When NaSal is incorporated into the micelle, this signal reveals that this proton is in a more electronegative surrounding than the other protons. Then, this proton is close to the micelle surface; NaSal is radially oriented in the micelle. To identify the weak PhazoBOO$^-$ signals in the spectra (c), (d), and (e), additional experiments of NMR varying temperature and correlated spectroscopy (^{1}H−^{1}H COSY) were developed.

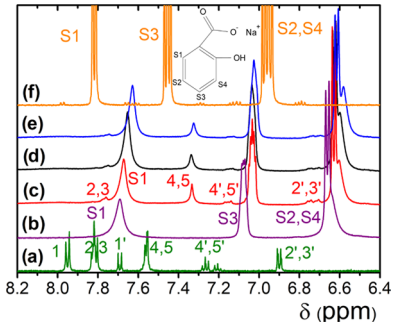

Figure 3. ^{1}H NMR spectra (D_2O/NaOD, pH = 12, 30 °C) of (a) pure PhazoBCOO$^-$; (b) CTAB-NaSal; CTAB/NaSal/ PhazoBCOO$^-$: (c) C_{AZO} = 10 mM, (d) C_{AZO} = 15 mM, (e) C_{AZO} = 20 mM; (f) pure NaSal. Signal numbering corresponds to protons shown in Figure 2, or when they begin with a letter S to protons in the inset of Figure 3.

Figure 4a presents the spectra for solutions of CTAB/NaSal/PhazoBCOO$^-$ (C_{AZO} = 15 mM) at different temperatures. As the temperature increases, the trans-PhazoBCOO$^-$ proton signals become sharper (Figure 2, protons: 1, 2, 3, 4, 5), and the NaSal signals are sharper with doublets and triplets. At 80 °C, there are no signals for the cis isomer, although at 25 and 30 °C, some low-intensity signals can be observed ($\delta \sim 7.2$ and $\delta \sim 6.8$ ppm); at high temperatures, the trans−cis isomerization is faster. The final identification for these signals

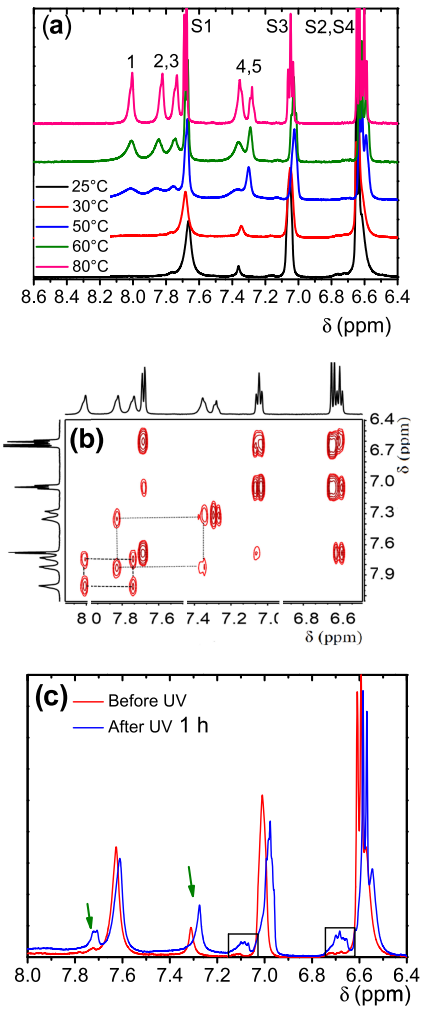

Figure 4. Spectra of CTAB/NaSal/PhazoBCOO$^-$ in deuterated water (C_{AZO} = 15 mM, pH = 12): (a) ^{1}H NMR spectra at different temperatures. (b) ^{1}H−^{1}H COSY spectrum (80 °C). (c) ^{1}H NMR spectra for the micellar solution before and after 1 h of UV irradiation (30 °C). Cis signals are inside squares, and trans signals are indicated by arrows.

DOI: 10.1021/acs.jpcb.9b07276
J. Phys. Chem. B 2019, 123, 9481−9490

is made using ^{1}H−^{1}H COSY at 80 °C, where coupling along three neighbor bonds can be observed.[33] In Figure 4b, there is a coupling (cross-peak) between H1 ($\delta \sim 8.0$ ppm) and H2 ($\delta \sim 7.7$ ppm), which are bound to the aromatic ring with a carboxylate. H3 ($\delta \sim 7.8$ ppm) and H4 ($\delta \sim 7.4$ ppm) are cross-peak-coupled, and H5 ($\delta \sim 7.3$ ppm) does not show any coupling, probably due to the resolution of the spectrum. These signals correspond to the protons of the phenyl group. The chemical shift of signals corresponding to the trans-azobenzene is not affected by temperature (Figure 4a); therefore, these signals can be assigned in the spectra obtained at lower temperatures (Figure 3c). The signals corresponding to H4 and H5 in Figure 3c moved to lower frequencies (less electronegative surrounding) and more shielded with respect to PhazoBCOO$^-$ in water. This seems to indicate that these protons are within the micelle surfactant tails. However, the H2 and H3 are less shielded (more electronegative surrounding) as they correspond to protons close to the surface of the WLM. The same occurs for the cis isomer. Consequently, PhazoBCOO$^-$ is incorporated into the cylindrical micelle. Figure 4c presents the spectra before and after the UV irradiation; they are similar. However, the signal intensity corresponding to both isomers increases. Cis signals are inside squares, and trans signals are indicated by arrows. The signals of the cis isomer increase due to the trans−cis transition. An unexpected increase of the trans isomer signals, as well as their slight shift, maybe due to small changes in the internal micelle structure because of the UV irradiation.

3.3. Mechanical Rheology. Figure 5a presents the normalized viscoelastic spectra for micellar solutions with PhazoBCOO$^-$ and their corresponding Cole−Cole plots (Figure 5c), before and after 1 h of UV irradiation. Irradiation is maintained during the rheological measurement. Figure 5b presents the results for the same solutions in Figure 5a, but here, NaCl was added (0.1 M). The micellar solution without PhazoBCOO$^-$ was also included for comparison in both figures. In general, the solutions are viscoelastic and Maxwellian, as shown in Figures 5c and S3 (Cole−Cole plots); this is typical behavior of WLMs. $G'(\omega)$ vs $G''(\omega)$ follow a semicircle at low and intermediate frequencies. Irradiation or NaCl addition does not seem to change the tubular structure. A similar result was reported by Pereira et al.[12] for WLMs made of CTAB/HSal with a molecular switch; they did not find a significant change in the viscoelastic spectra after UV irradiation; they suspected that the micellar length was reduced. Micellar solutions are more viscous than elastic at low frequencies. On the contrary at higher frequencies, after the crossing point between $G'(\omega)$ and $G''(\omega)$ curves, the solutions are more elastic. The corresponding τ values for the frequency of the crossing point, ω_c, are ~32.5−0.16 s and $G_o \sim$ 17−57 Pa (see Figures S1a,b and S2a,b). However, there are important points to be noted: (1) the spectra move to higher frequencies, increasing the quantity of PhazoBCOO$^-$ added (see Figures S1a and S2a). However, if the spectra are normalized, their behavior is very similar (Figure 5a,b). Differences in the position of the crossing points are small, although the position of G''_{min} decreases notoriously at low concentrations of the azo-compound. At higher concentrations of PhazoBCOO$^-$, G''_{min} does not vary significantly (dashed arrows in Figure 5a,b). Therefore, the ratio of the lengths l_e/L_c must increase as PhazoBCOO$^-$ is incorporated in micelles; we will go back to this issue later. For the solution with C_{AZO} = 10 mM, with or without NaCl, the spectra move to lower

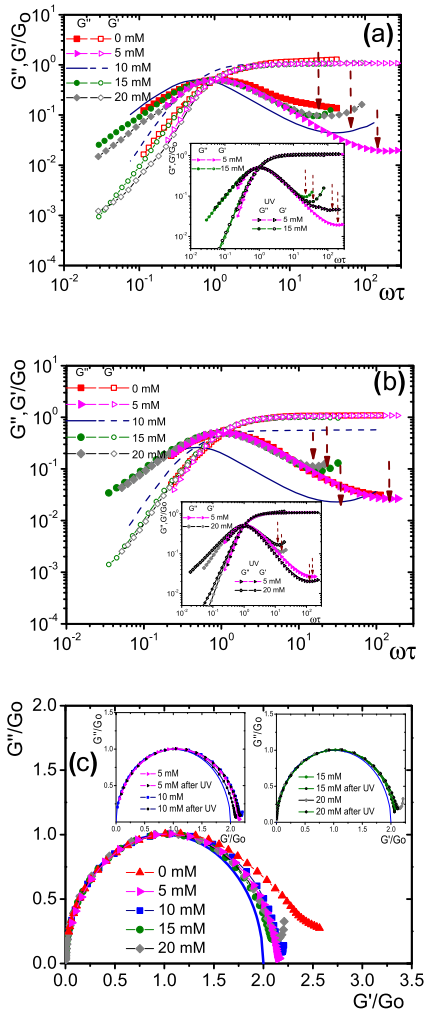

Figure 5. (a) $G'(\omega)/G_o$ and $G''(\omega)/G_o$ vs $\omega\tau$ of several micellar solutions as a function of C_{AZO}, without the addition of NaCl, before UV irradiation at T = 30 °C. (b) Same plot as in (a) also as a function of C_{AZO} and before UV irradiation at T = 30 °C, but after the addition of NaCl. The insets in (a, b): viscoelastic spectra for two micellar solutions presented as in the main figures, before and after UV irradiation, without and with added NaCl, respectively. (c) Cole−Cole plots for the spectra presented in (a); insets: comparison of the Cole−Cole plots before and after UV irradiation for the solutions in the main figure.

frequencies not following the concentration pattern of the other cases. (2) Viscoelastic spectra of the micellar solutions are slightly modified by UV irradiation (insets of Figures 5a,b, S1b and S2b). (3) The addition of PhazoBCOO$^-$ seems to improve the Maxwellian behavior at lower and intermediate frequencies, as shown by the Cole−Cole plots in Figure 5c; the same behavior is shown by the UV-irradiated solutions (inset of Figure 5c). The addition of NaCl to the micellar solutions improves even more the Maxwellian behavior, no matter if they are UV-irradiated (insets of Figure S3) or not irradiated (Figure S3).

Figure 6a presents the variation of the relaxation time with the PhazoBCOO$^-$ concentration for micellar solutions without and with NaCl. Curiously, an initial addition of the azo-compound increases τ significantly, but a successive addition of PhazoBCOO$^-$ notoriously decreases τ, even below the level of the micelles without the chromophore. This behavior is the same for uncharged micelles with or without UV irradiation;

DOI: 10.1021/acs.jpcb.9b07276
J. Phys. Chem. B 2019, 123, 9481−9490

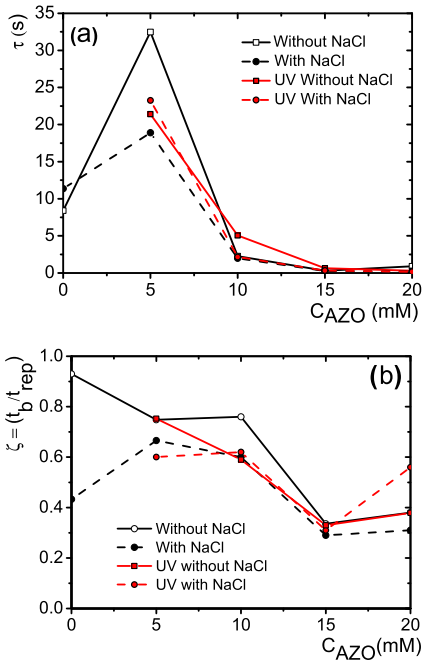

Figure 6. Time constants obtained from the viscoelastic spectra at 30 °C. (a) Relaxation time vs C_{AZO} (b) ζ vs C_{AZO}. Lines are guides to the eye.

the addition of NaCl does not make a big difference. Figure S4 presents the characteristic reptation time, t_{rep}, and the characteristic breaking−reforming time, t_b, as a function of the PhazoBCOO$^-$ concentration for the micellar solutions without and with NaCl. We followed the method given by Turner and Cates[6] for calculating these characteristic times. In a Cole−Cole plot $(G''(\omega)/G_0$ vs $G'(\omega)/G_0)$, we fit a semicircle to the experimental points to the left of the maximum in $G''(\omega)/G_0$. Then, a tangent line from the experimental data to high-frequency $G''(\omega)/G_0 = 0$, with gradient −1, gives the diameter of the fitted semicircle (DFS). From the plot DFS vs $\overline{\zeta}$ presented in Figure 2 of ref 6, $\overline{\zeta} = t_b/\tau$ is evaluated and using $\tau \approx \sqrt{t_b t_{rep}}$, a value for t_{rep} can be estimated. Both characteristic times increase with the initial addition of PhazoBCOO$^-$, but the successive addition of PhazoBCOO$^-$ significantly decreases both times. Figure 6b shows the ratio of both characteristic times, $\zeta = t_b/t_{rep}$,[34] which indicates how good the Maxwell model is ($\zeta < 1$) for describing different micelle solutions (perfect when $\zeta \ll 1$). We observe the following: (1) micelles without the addition of NaCl and PhazoBCOO$^-$ follow the model in a limited way because t_b and t_{rep} are of the same order. (2) The addition of PhazoBCOO$^-$ reduces ζ improving the Maxwellian behavior; this agrees with the results of Figures 5c and S3. (3) Similar behavior is observed for irradiated micellar solutions. UV irradiation does not change the behavior of ζ except at C_{AZO} = 20 mM with NaCl added, where ζ increases although the fluid is still Maxwellian. (4) In general, the addition of NaCl to WLMs promotes the increase of the micellar contour length due to a discharge process, improving the value of ζ. Without the azo-compound, the ζ value for micelles in brine is quite good. The same trend is observed when the chromophore is added since ζ decreases as the concentration of PhazoBCOO$^-$ increases.

The flow curves η (viscosity) vs $\dot{\gamma}$ of the micellar solutions without and with NaCl are shown in Figures 7a and S5,

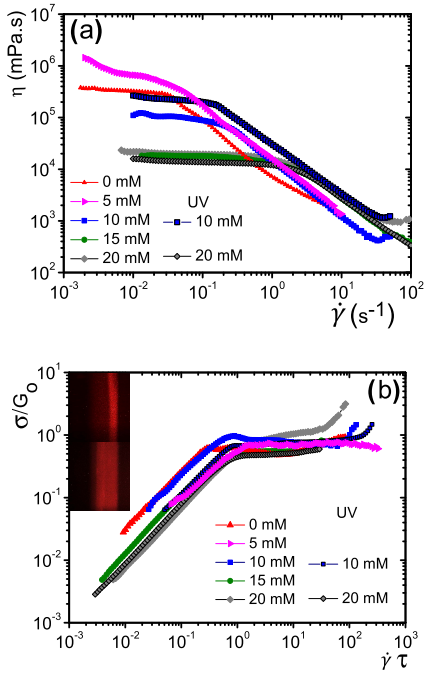

Figure 7. (a) Viscosity of the micellar solution vs $\dot{\gamma}$ for different C_{AZO} values, without the addition of NaCl, before and after UV irradiation, at 30 °C. (b) σ vs $\dot{\gamma}$ corresponding to the concentrations in (a); inset: shear bands observed with the aid of a sheet of light (the color is artificial) for C_{AZO} = 10 mM without NaCl; the upper image at $\dot{\gamma}\tau = 4$ and the lower image at $\dot{\gamma}\tau = 58$.

respectively. In both cases, at low $\dot{\gamma}$ values, η is approximately constant or slightly thinning. However, at specific values of $\dot{\gamma} = \dot{\gamma}_1$, all of the solutions significantly shear thin with almost the same slope. Here, on the average, when the switchable molecule is present, we found $\eta \sim \dot{\gamma}^{-\kappa 1}$, where $\kappa 1$ = 0.96−1 with or without adding NaCl. As C_{AZO} increases, $\dot{\gamma}_1$ increases and kinks become sharper. At C_{AZO} = 5 mM, at low shear rates, η is larger than the micellar solution without the azo-compound. This agrees with the increase of τ observed in Figure 6a for this solution compared to the one without the azo-compound. UV irradiation does not make a significant difference. At C_{AZO} = 10 mM, viscosities are lower than in the micellar solution without the azo-compound; this agrees with the τ values obtained in Figure 6a. UV light irradiation slightly increases the viscosities in agreement with the values of τ for these solutions. The curves for the normalized viscosities almost collapse on a single curve (see Figures S6a and S7a), no matter if NaCl is added. As PhazoBCOO$^-$ concentration increases, the viscosity at low shear rates decreases. In Figure 7b and the inset of Figure S5, we present the normalized shear stress, σ/G_0 vs $\dot{\gamma}$, for both cases without and with NaCl. For Weissenberg numbers, $Wi = \tau\dot{\gamma} \geq 1$, the flow curves are almost horizontal. Here, when the photoswitchable molecule is present, we found $\sigma \sim \dot{\gamma}^{\kappa 2}$, with $\kappa 2 = -0.04 \sim 0$ and $0.04 \sim 0$, with and without NaCl, respectively. This is a fingerprint indicating that the elastic component of the flow is of the same order of inertia, and where shear banding transitions occur in WLM solutions. The inset of Figure 7b shows an example of shear banding with the aid of a sheet of light.[35] Therefore, the incorporation of the PhazoBCOO$^-$ in the micelles preserves

DOI: 10.1021/acs.jpcb.9b07276
J. Phys. Chem. B 2019, 123, 9481−9490

shear banding in agreement with what is observed in Figure 1e. In Figures S6b and S7b, the σ vs $\dot{\gamma}$ curves are presented without normalization.

3.4. Microrheology. The selection of the used tracer microspheres falls on the index of refraction difference between microspheres and dispersive medium. The larger is the difference, the better is the optical resolution obtained. Although the typical microspheres used to perform DWS experiments are negatively charged polystyrene particles, our WLM suspensions made with these particles are not stable for all of the C_{AZO} values. For this reason, we used microspheres with amino-functionalized surfaces that are neutral at the high pH of our suspensions. Micellar suspensions with these particles are stable in a broader concentration range. Figures 8a and S8 show the typically measured curves of $\langle \Delta r^2(t) \rangle$ vs t

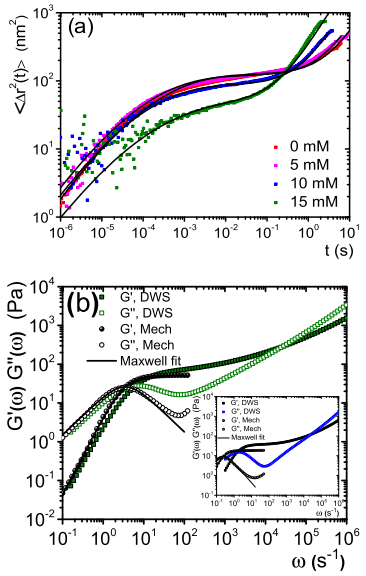

Figure 8. (a) MSD vs time of 800 nm microspheres (NH_2 surface functionalization) in the micellar solution with different concentrations of PhazoBCOO$^-$, at T = 30 °C, without NaCl. R = 0.5 and [CTAB] = 0.080 M. Lines are the best-fits for the Bellour et al. model. (b) Viscoelastic spectra of the micellar solution at C_{AZO} = 15 mM; the inset at 10 mM, both at 30 °C (R = 0.5 and [CTAB] = 0.080 M). Lines are the best-fits to the Maxwell model for the mechanical rheological measurements.

for microspheres of a diameter of 800 nm dispersed in the WLM solution at different concentrations of PhazoBCOO$^-$, without and with NaCl (C_{CTAB} = 80 mM, R = 0.5, and T = 30 °C) spanning over 7 orders of magnitude in time. The $\langle \Delta r^2(t) \rangle$ curves come from the numerical inversion of the correlation functions obtained with DWS experiments. They are fitted to the model proposed by Bellour et al.[22] as described above, leaving δ, D_m, D_o, and α as free parameters. We observe three different regimes of motion, which are shared by all micellar solutions reported previously. At short times, there is a regime where $\langle \Delta r^2(t) \rangle$ is almost a linear function of time: $\langle \Delta r^2(t) \rangle = 6D_o t$; here, D_o is the local diffusion coefficient. At intermediate times, $\langle \Delta r^2(t) \rangle$ remains almost constant where the curve shows a plateau. Here, according to the model, the motion of Brownian particles is harmonically bound around a stationary mean position, at time scales smaller than the characteristic stress relaxation time τ. The amplitude of the particle motion, the cage size δ, measures the average distance at which particles are momentarily trapped before the network relaxes to permit them to continue its displacement, and it is related to the elastic modulus G_o ($6\delta^2 = k_BT/[\pi r_o G_o]$). Then, at longer times, $\langle \Delta r^2(t) \rangle$ is again a linear function of time, $\langle \Delta r^2(t) \rangle = 6D_m t$, as proposed in eq 2; D_m is mainly determined by the long-time viscosity of the solutions η_m through $D_m = k_BT/6\pi r_o \eta_m$. Dynamics of the microspheres exhibit a broad time relaxation spectrum at the plateau onset time; this leads to include a parameter α as given by eq 2.

The MSD curves are quite similar without and with NaCl, Figures 8a and S8, respectively. The curves shift downwards as we increase the PhazoBCOO$^-$ concentration. At short times, $\langle \Delta r^2(t) \rangle$ measurements for the WLMs with PhazoBCOO$^-$ are noisy, despite a long time of measurement under the laser beam (~3 h). At these short times, we expect that the diffusion of microspheres must be close to its value in water. Our measured values are indeed close to the diffusion $D_o = 6.93 \times 10^{-13}$ m^2/s, at 30 °C, in pure water. For WLM solutions without both NaCl and PhazoBCOO$^-$, $6\delta^2 \sim 125$ nm^2. If NaCl is added, $6\delta^2 \sim 90$ nm^2. The cage size is smaller when the PhazoBCOO$^-$ concentration increases (120 nm^2 at C_{AZO} = 5 mM to 50 nm^2 at C_{AZO} = 15 mM), and if NaCl is added, the $6\delta^2$ values are even smaller. The average value of $6\delta^2$ found in other WLM network systems is of the same order of magnitude as those found here. This is the case of $CTAC_7SO_3$ where $6\delta^2 \sim 51$ nm^2 [22] and smaller than in the case of TDPS/SDS in salty water where $6\delta^2$ goes from 200 to 400 nm^2 depending on the type of added salt.[36] The average value for α in the WLM solutions is $\alpha \sim 0.3$. The smaller α, the larger is the time relaxation spectrum (α = 1 indicates monoexponential relaxation). On average, α values found in this work are of the same order as those α values for WLM solutions of TDPS/SDS[36] and $CTAC_7SO_3$.[22]

From the $\langle \Delta r^2(t) \rangle$ vs t curves obtained above, the elastic and the viscous components of $G^*(\omega)$ are evaluated, using the Laplace transform and analytic continuity.[18] Examples of $G'(\omega)$ and $G''(\omega)$ are presented in Figures 8b and S9a for micellar solutions without NaCl and in Figure S9b with NaCl. In some cases, data obtained with the mechanical rheometer are also presented at low and intermediate frequencies. The moduli obtained by DWS and mechanical rheometry are reasonably similar, although not equal. In a general way, it has been noted that at shorter τ values, the deviation between both methods is more substantial.[36] It has been suggested that hydrotrope salt ions in solution could be responsible for this deviation, but this suggestion is not supported by a later experimental work, as well as it has been suggested that in an oscillatory shear experiment, the real and imaginary parts of $G^*(\omega)$ are determined from the amplitude and phase shift of the response signal. Such a phase analysis is much more accurate than the DWS data treatment, where $\langle \Delta r^2(t) \rangle$ is measured in time−space. Residual effects of the polynomial fitting can produce small deviations in $G'(\omega)$ and $G''(\omega)$. Then, we expect a larger error in the calculation of the crossing point. DWS microrheology reaches a bandwidth far beyond the conventional rheometry, allowing us to observe two crossovers in $G^*(\omega)$, as presented in Figure 8b. Probe size and solvent inertial effects are negligible up to frequencies of $\omega > 10^6$ s^{-1}. At high frequencies as mentioned in the Experimental Section, the micelles can be regarded as semiflexible chains, where $G^*(\omega)$ exhibits a power-law behavior with an exponent change as frequency increases (from $\nu \sim 5/9$ to $\nu \sim 3/4$) (see Figure S10); the change occurs at frequency ω_0.[23] Another important

DOI: 10.1021/acs.jpcb.9b07276
J. Phys. Chem. B 2019, 123, 9481−9490

feature to be pointed out is related to the local minimum of $G''(\omega)$ after the first crossover denoted by G''_{min}, which is usually better defined in DWS microrheology than in mechanical rheometry. With $G^*(\omega)$ obtained with DWS, it is possible to evaluate the characteristic lengths of the WLM network of the system, using approximate relations coming from theory, as described in the Experimental Section. Note that $G''_{min}/G_0 < 0.3$ for most of our micellar solutions; this ratio produces relatively reliable values for l_e/L_c.[25]

Figure 9a presents L_c vs C_{AZO}, without and with NaCl. We observe that without the chromophore (C_{AZO} = 0 mM), NaCl

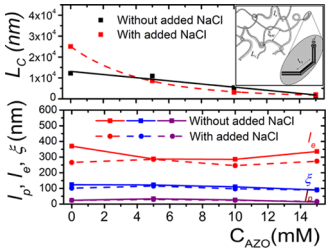

Figure 9. Micelle length scales as a function of C_{AZO} at 30 °C: (a) total contour length of WLMs without NaCl (the line is an exponential line) and with NaCl (the line is a straight line). The inset modified from B. A. Schubert, E. W. Kaler, and N. J. Wagner, Langmuir 2003, 19, 4079. (b) Persistence and entanglement lengths, as well as mesh size; here, lines are guides to the eye.

addition increases, as expected, the total contour length of the micelles because the surface is discharged due to a screening of the charged groups on the WLM surface. As the solution is more abundant in PhazoBCOO$^-$, the micelles become smaller. This effect prevents the increase of the chromophore concentration within the micelle. The modification of L_c after NaCl or azo-compound addition is related to a change in the micelle scission energy, preventing or allowing the formation of end caps, which are competing with the mixing entropy; the balance determines L_c.[37,38] When NaCl is added, the dependence of L_c on C_{AZO} exponentially decays, and when NaCl is not added, the relation decays linearly. Figure 9b presents how l_e, ξ, and l_p vary when PhazoBCOO$^-$ is added; the change is not significant, neither with NaCl added. In Table 1, there is a comparison among several determined length scales in WLM systems. L_c measured in this system (∼1.40−25 μm) are in the same range as those in other previously reported WLM systems. Our l_p ∼ 12.6−33.6 nm is not far from the l_p values obtained for WLMs by other authors in different systems. Our system is in the loose entanglement regime, because α_e values are much larger than 2. The mesh size in our micellar solutions is ξ ∼ 88−124 nm, which is of the same order of magnitude than in other systems. The entanglement lengths in our WLMs are in the range of l_e ∼ 246−369 nm; in some cases, our values are larger than in other micelle solutions.

4. CONCLUSIONS

WLM solutions made of CTAB/NaSal accept up to 20 mM of PhazoBCOO$^-$, preserving the tubular structure, although the micelle is modified. The larger is the concentration of the embedded azobenzene, the smaller is the length of the micelles; the other scale lengths of the WLM network do not substantially vary. The addition of NaCl to the system increases the micellar contour length, but it does not modify other length scales of the micellar network in a significant way. The micellar solution viscosity decreases as PhazoBCOO$^-$ concentration increases, and it presents shear banding. The viscoelastic spectra are modified, but when they are properly rescaled, they can be superimposed. The addition of PhazoBCOO$^-$ makes the fluids more Maxwellian, mainly when NaCl is also added.

We demonstrated that a chromophore (PhazoBCOO$^-$) susceptible to light-induced trans−cis isomerization could be inserted in cylindrical micelles made of CTAB/NaSal. However, the response of the system to UV radiation is not very significant. The chromophore lowers the scission energy, and, consequently, the total contour length of the micelles decreases. PhazoBCOO$^-$ concentration in the micelles is not enough to make the system a photosensitive material with great possibilities for rheological use as in other cases.[10]

The general trend in the ongoing research is to determine the light-responsive performance of a chromophore embedded in micelles to modify the rheological behavior.[9,10,13,30] However, we are more interested to understand how chromophore−micelle interaction is. This report presents the first of a series of studies to determine how the interaction between WLMs and photoswitchable molecules is, particularly when these molecules have a different chemical nature or configuration. As we will present shortly, in some cases, the cis conformation can be expelled from the micelle on UV irradiation, and in others, the photoactive molecules can modify the structure of the micellar solution acting on the surface of the WLMs. This understanding provides a physicochemical insight into why particular rheological behavior is observed in micellar solutions after UV irradiation. This knowledge can be used to design better light-responsive systems.

Table 1. Comparison Among Several Determined Length Scales in WLM Systems

system	T (°C)	L_c (μm)	l_p (nm)	l_e (nm)	ξ (nm)	α_e	references
CTAB/NaSal, R = 0.4	22	27.82	45	171.4	100.4	3.8	18[a]
CPyCl/NaSal, R = 0.5−5	20−40		26−29				39
CTAB (with nonpenetrating ions Br^-, NO_3^-, ClO_3^-)			25−41	71.5−86.3	50−64		40[a]
TDPS/SDS, R = 0.5 [NaCl] = 0.5 M	20−30	7.2−28	30.5−31.1	328−463	126.8−157.3	10.7−14.9	36[a]
CPyCl/NaSal, R = 0.6	20−40		31−34				23
present work without NaCl	30	1.4−12	12. 6−33.6	285−369	90.5−124	8−26	
present work with NaCl = 0.1 M	30	1.9−25	16.3−29.6	246−286	88−115	9.6−16.7	

[a]Original data was modified to use the corrected formulas given in the text.

DOI: 10.1021/acs.jpcb.9b07276
J. Phys. Chem. B 2019, 123, 9481−9490

■ ASSOCIATED CONTENT

Supporting Information

The Supporting Information is available free of charge on the ACS Publications website at DOI: 10.1021/acs.jpcb.9b07276.

Viscoelastic spectra of system; Cole−Cole plots of several micellar solutions; time constants obtained from the viscoelastic spectra; viscosity vs shear rate; MSD vs time; viscoelastic spectra of the micellar solution (PDF)

■ AUTHOR INFORMATION

Corresponding Author

*E-mail: rolandoc@fisica.unam.mx.

ORCID

Antonio Tavera-Vázquez: 0000-0001-8304-2123

Anna Kozina: 0000-0002-4287-2953

Rolando Castillo: 0000-0001-6331-0311

Present Address

§Institute for Molecular Engineering, The University of Chicago, Chicago, Illinois 60637, United States (A.T.-V.).

Notes

The authors declare no competing financial interest.

■ ACKNOWLEDGMENTS

The authors acknowledge the financial support from DGAPA-UNAM (IN 106218). The authors thank LURMN at IQ-UNAM with funds of CONACYT (0224747) for the NMR measurements, S. Ramos for his technical help, and S. Tehuacanero-Cuapa for his help in the acquisition of SEM images.

■ REFERENCES

(1) Dreiss, C. A. Wormlike micelles: where do we stand? Recent developments, linear rheology and scattering techniques. *Soft Matter* **2007**, *3*, 956−970.

(2) Ezrahi, S.; Tuval, E.; Aserin, A. Properties, main applications and perspectives of worm micelles. *Adv. Colloid Interface Sci.* **2006**, *128−130*, 77−102.

(3) Yang, J. Viscoelastic wormlike micelles and their applications. *Curr. Opin. Colloid Interface Sci.* **2002**, *7*, 276−281.

(4) Schöbel, J.; Karg, M.; Rosenbach, D.; Krauss, G.; Greiner, A.; Schmalz, H. Patchy wormlike micelles with tailored functionality by crystallization-driven self-assembly: A versatile platform for mesostructured hybrid materials. *Macromolecules* **2016**, *49*, 2761−2771.

(5) Dan, N.; Safran, S. A. Functions and end-caps in self-assembled non-ionic cylindrical micelles. *Adv. Colloid Interface Sci.* **2006**, *123*, 323−331.

(6) Turner, M.; Cates, M. Linear viscoelasticity of living polymers: a quantitative probe of chemical relaxation times. *Langmuir* **1991**, *7*, 1590−1594.

(7) Chu, Z.; Dreiss, C. A.; Feng, Y. Smart wormlike micelles. *Chem. Soc. Rev.* **2013**, *42*, 7174−7203.

(8) Wang, A.; Shi, W.; Huang, J.; Yan, Y. Adaptive soft molecular self-assemblies. *Soft Matter* **2016**, *12*, 337−357.

(9) Bi, Y.; Wei, H.; Hu, Q.; Xu, W.; Gong, Y.; Yu, L. Wormlike micelles with photoresponsive viscoelastic behavior formed by surface active Ionic liquid/azobenzene derivative mixed solution. *Langmuir* **2015**, *31*, 3789−3798.

(10) Oh, H.; Ketner, A. M.; Heymann, R.; Kesselman, E.; Danino, D.; Falvey, D. E.; Raghavan, S. R. A simple route to fluids with photoswitchable viscosities based on a reversible transition between vesicles and wormlike micelles. *Soft Matter* **2013**, *9*, 5025−5033.

(11) Li, L.; Yang, Y.; Dong, J.; Li, X. Azobenzene dye induced micelle to vesicle transition in cationic surfactant aqueous solutions. *J. Colloid Interface Sci.* **2010**, *343*, 504−509.

(12) Pereira, M.; Leal, C.; Parola, A.; Scheven, U. Reversible photorheology in solutions of cetyltrimethylammonium bromide, salicylic acid, and trans-2,4,4′-trihydroxychalcone. *Langmuir* **2010**, *26*, 16715−16721.

(13) Sakai, H.; Orihara, Y.; Kodashima, H.; Matsumura, A.; Ohkubo, T.; Tsuchiya, K.; Abe, M. Photoinduced reversible change of fluid viscosity. *J. Am. Chem. Soc.* **2005**, *127*, 13454−13455.

(14) Tu, Y.; Chen, Q.; Shang, Y.; Teng, H.; Liu, H. Photoresponsive behavior of wormlike mocelles constructed by Gemini surfactant 12-3-12. 2Br- and different cinnamate derivatives. *Langmuir* **2019**, *35*, 4634−4645.

(15) Tu, Y.; Ye, Z.; Lian, C.; Shang, Y.; Teng, H.; Liu, H. UV-responsive behavior of multistate and multiscale self-assemblies constructed by gemini surfactant 12-3-12.2 Br- and trans-o-methoxy-cinnamate. *Langmuir* **2018**, *34*, 12990−12999.

(16) Tu, Y.; Gao, M.; Teng, H.; Shang, Y.; Fang, B.; Liu, H. A gemini surfactant-containing suystem with abundant self-assembly morphology and rheological behaviours tunable by photoinduction. *RSC Adv.* **2018**, *8*, 16004−16012.

(17) Mason, T. G. Estimating the viscoelastic moduli of complex fluids using the generalized Stokes−Einstein equation. *Rheol. Acta* **2000**, *39*, 371−378.

(18) Galvan-Miyoshi, J.; Delgado, J.; Castillo, R. Diffusing wave spectroscopy in Maxwellian fluids. *Eur. Phys. J. E* **2008**, *26*, 369−377.

(19) Prahl, S. A.; Van Gemert, M. J.; Welch, A. J. Determining the optical properties of turbid media by using the adding-doubling method. *Appl. Opt.* **1993**, *32*, 559−568.

(20) Inverse Adding Doubling. http://omlc.ogi.edu/software/iad/index.html (accessed June 2, 2017).

(21) Sarmiento-Gomez, E.; Morales-Cruzado, B.; Castillo, R. Absorption effects in diffusing wave spectroscopy. *Appl. Opt.* **2014**, *53*, 4675−4682.

(22) Bellour, M.; Skouri, M.; Munch, J. P.; Hébraud, P. Brownian motion of particles embedded in a solution of giant micelles. *Eur. Phys. J. E* **2002**, *8*, 431−436.

(23) Willenbacher, N.; Oelschlaeger, C.; Schopferer, M.; Fischer, P.; Cardinaux, F.; Scheffold, F. Broad bandwidth optical and mechanical rheometry of wormlike micelle solutions. *Phys. Rev. Lett.* **2007**, *99*, No. 068302.

(24) Zou, W.; Larson, R. G. A mesoscopic simulation method for predicting the rheology of semi-dilute wormlike micellar solutions. *J. Rheol.* **2014**, *58*, 681−721.

(25) Granek, R.; Cates, M. E. Stress relaxation in living polymers: Results from a Poisson renewal model. *J. Chem. Phys.* **1992**, *96*, 4758−4767.

(26) Granek, R. Dip in G″(ω) of polymer melts and semidilute solutions. *Langmuir* **1994**, *10*, 1627−1629.

(27) Das, N. C.; Cao, H.; Kaiser, H.; Warren, G. T.; Sokol, P. E.; Gladden, J. R. Shape and size of highly concentrated micelles in CTAB/NaSal solutions by small angle neutron scattering (SANS). *Langmuir* **2012**, *28*, 11962−11268.

(28) Yang, D.; Zhao, J. Light-responsive organofluid based on reverse worm-like micelles formed from an equi-charged, mixed, anionic gemini surfactant with an azobenzene spacer and a cationic conventional surfactant. *Soft Matter* **2016**, *12*, 4044−4051.

(29) Lu, Y.; Zhou, T.; Fan, Q.; Dong, J.; Li, X. Light-responsive viscoelastic fluids based on anionic wormlike micelles. *J. Colloid Interface Sci.* **2013**, *412*, 107−111.

(30) Takahashi, Y.; Yamamoto, Y.; Hata, S.; Kondo, Y. Unusual viscoelasticity behaviour in aqueous solutions containing a photo-responsive amphiphile. *J. Colloid Interface Sci.* **2013**, *407*, 370−374.

(31) Zhao, M.; Gao, M.; Dai, C.; Zou, C.; Yang, Z.; Wu, X.; Liu, Y.; Wu, Y.; Fang, S.; Lv, W. Investigation of novel triple-responsive wormlike micelles. *Langmuir* **2017**, *33*, 4319−4327.

(32) Shikata, T.; Hirata, H.; Kotaka, T. Micelle formation of detergent molecules in aqueous media. 2. Role of free salicylate ions on viscoelastic properties of aqueous cetyltrimethylammonium bromide-sodium salicylate solutions. *Langmuir* **1988**, *4*, 354−359.

DOI: 10.1021/acs.jpcb.9b07276
J. Phys. Chem. B 2019, 123, 9481−9490

(33) Appiah, C.; Siefermann, K.; Jorewitz, M.; Barqawi, H.; Binder, W. H. Synthesis and characterization of new photoswitchable azobenzene-containing poly(ε-caprolactones). *RSC Adv.* **2016**, *6*, 6358−6367.
(34) Cates, M. Reptation of living polymers: dynamics of entangled polymers in the presence of reversible chain-scission reactions. *Macromolecules* **1987**, *20*, 2289−2296.
(35) Delgado, J.; Castillo, R. Shear-induced structures formed during thixotropic loops in dilute worm-micelle solutions. *J. Colloid Interface Sci.* **2007**, *312*, 481−488.
(36) Sarmiento-Gomez, E.; Lopez-Diaz, D.; Castillo, R. Microrheology and characteristic lengths in wormlike micelles made of a zwitterionic surfactant and SDS in brine. *J. Phys. Chem. B* **2010**, *114*, 12193−12202.
(37) Jiang, H.; Vogtt, K.; Thomas, J.; Beaucage, G.; Mulderig, A. Enthalpy and entropy of scission in wormlike micelles. *Langmuir* **2018**, *34*, 13956−13964.
(38) Mitrinova, Z.; Tcholakova, S.; Denkov, N. Control of surfactant solution rheology using medium-chain cosurfactants. *Colloids Surf., A* **2018**, *537*, 173−184.
(39) Oelschlaeger, C.; Schopferer, M.; Scheffold, F.; Willenbacher, N. Linear-to-branched micelles transition: A rheometry and diffusing wave spectroscopy (DWS) study. *Langmuir* **2009**, *25*, 716−723.
(40) Oelschlaeger, C.; Suwita, P.; Willenbacher, N. Effect of counterion binding efficiency on structure and dynamics of wormlike micelles. *Langmuir* **2010**, *26*, 7045−7053.

DOI: 10.1021/acs.jpcb.9b07276
J. Phys. Chem. B 2019, 123, 9481−9490